Partial Rebound of Molten-Metal Droplets Impacting on Solid Substrates

Constantine M. Megaridis, Kevin Boomsma, and Ilker S. Bayer
Dept. of Mechanical and Industrial Engineering, University of Illinois at Chicago, Chicago, IL 60607

DOI 10.1002/aic.10123
Published online in Wiley InterScience (www.interscience.wiley.com).

This study investigates droplet/wall impact events resulting in partial rebound, an overlooked regime between deposition and splash. Because of its relevance to the microelectronics manufacturing industry, high-purity 63%Sn–37%Pb molten solder is used. The target wall consists of a smooth, flat, unyielding silicon substrate. Droplet diameters range from 0.7 to 1.4 mm, and impact velocities from 0.7 to 1.4 m/s. These conditions correspond to Re = O(1000), We = O(10), Fr = O(10–100), Bo = O(0.1), and Oh = O(10^{-3}). High-speed imaging is performed to determine droplet lateral spread and apparent contact angles, and examine how these quantities affect the impact outcome (deposition vs. partial rebound). The results indicate that partial rebound is favored by higher impact velocities and smaller droplet diameters. A recent rebound model is evaluated as a predictive tool for the impact outcome in this transition impact regime. In addition, three existing correlations are evaluated in terms of their ability to predict the current experimental data on droplet maximum spread. © 2004 American Institute of Chemical Engineers *AIChE J,* 50: 1356–1363, 2004
Keywords: molten-metal, droplet, impact, recoil, partial rebound

Introduction

The impact of liquid droplets on solid surfaces is associated with a variety of visually rich fluid-transport phenomena, which have fascinated humans and attracted scientific attention dating back to the late 19th century (Worthington, 1876). One of the major issues studied over the years has been the outcome of the droplet/wall collision, which may result in deposition upon impact, rebound, or splash. The term *rebound* is used herein to indicate that all (complete rebound) or a portion (partial rebound) of the liquid detaches from the wall at any stage after initial contact. The review by Rein (1993) has provided a thorough investigation of the influence of several parameters, ranging from the properties of the drop or the solid surface, to the properties of the fluid surrounding the droplet. More recently, Rioboo et al. (2001) provided a qualitative analysis of the various outcomes of drop impact on solid surfaces, which are characterized by different roughness and wettability. A first classification of these outcomes, in terms of splash, rebound, partial rebound, or deposition, was presented therein. Despite considerable progress made recently, primarily with detailed numerical models, fundamental understanding of certain aspects of fluid flow when drops impinge on a solid surface remains yet incomplete.

Several models have been presented in the literature to predict the maximum droplet spreading diameter. Most of these models [see, for example, Fukai et al. (1998) and references cited therein] considered conventional fluids, and demonstrated agreement with experimental results under certain impact conditions. Aziz and Chandra (2000) presented an energy conservation model, which performed well for *molten*-metal droplets solidifying upon impact on a cooler wall. The importance of maximum spreading in the outcome of the drop/wall impact was recognized by Mao et al. (1997b), who developed a model to predict the tendency to rebound as a function of maximum spread and static contact angle. The model formulation was based on the realization that a droplet possesses the maximum surface energy for recoil and rebound at its maximum spread. In a follow-up study (Mao et al., 1997a), the same investigators

Correspondence concerning this article should be addressed to C. M. Megaridis at cmm@uic.edu.

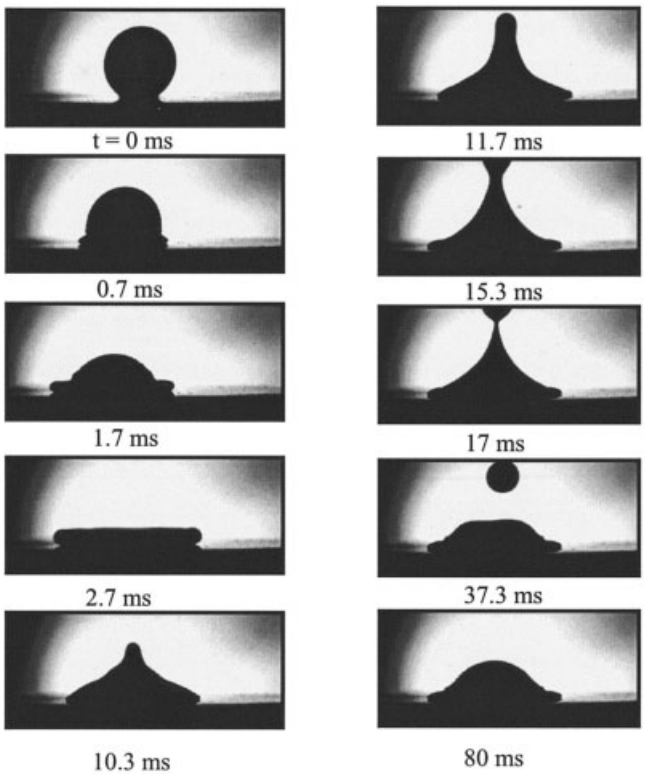

Figure 1. Experimental images obtained by high-speed video (3,000 fps) when a 1.34-mm molten Sn/Pb solder droplet impacted orthogonally at 1.3 m/s onto a flat smooth Si substrate.

Note the breakup and subsequent reattachment of the secondary droplet during the recoiling after impact.

considered nonisothermal impact of molten sodium nitrate on cool substrates, and reported that in cases where the effect of solidification is insignificant, the drop tendency to rebound could also be predicted using their isothermal model.

The present study concentrates on a narrow range of molten-metal–droplet/wall impact conditions, which result in *partial* rebound (or breakup) as seen in Figure 1. This figure demonstrates a temporal sequence of experimental images obtained by high-speed digital videography when a 1.34-mm-diameter Sn/Pb solder droplet impacted with a velocity of 1.3 m/s on a flat, smooth silicon substrate. The pinchoff seen during the first recoiling cycle in Figure 1 is of particular significance to solder jet technology, which relies on ink-jet printing principles to create and place monodisperse arrays of miniature (30 to 120 μm in diameter) molten-solder droplets on substrates (Hayes et al., 1993). The droplets solidify *after* impact, thus forming metal bump deposits, which are subsequently used for the flip-chip bonding of electronic components on the substrate. Droplet breakup events, such as the one seen in Figure 1, are not desirable in solder jet technology because they may cause random deposition of solder volumes in areas of the substrate where they are unwanted. It is thus important to identify a reliable means of predicting the outcome of drop/wall impact using materials relevant to solder jet technology. Furthermore, the need to predict droplet impact outcome is not limited only to microelectronic manufacturing, but extends to other technological applications, such as coating and deposition processes (Bergeron et al., 2000; Klein, 2000). The partial breakup mode seen in Figure 1 occurs in the transition from deposition (low impact energy) to splash (high impact energy), the latter corresponding to the ejection of multiple droplets upon collision (Mundo et al., 1995). It is emphasized, however, that the splashing regime is not within the scope of the present study.

Although images of partial rebound events, such as those seen in Figure 1, have been reported previously in the literature (Rioboo et al., 2001, 2002; Waldvogel et al., 1998), the fluid transport phenomena in this regime have not attracted much attention in other investigations of droplet/wall impact. It is the main objective of this study to interrogate this impact regime using molten-metal droplets, and examine whether the rebound model of Mao et al. (1997b) is capable of predicting the partial rebound outcome. Also, a secondary goal of this study is to examine whether existing correlations of droplet maximum spread agree with the experimental data for impact velocities about 1 m/s and impact diameters of about 1 mm [Reynolds number (Re) = 2000–6000; Weber number (We) = 10–60].

Experimental Procedures

The experimental apparatus consisted of three major components: droplet generator, environmental chamber, and visualization system. A brief description of each component is given in the following. Further details of the experimental setup are provided in Boomsma (1999).

A thin-walled passivated stainless steel cylinder with an orifice diameter of 0.62 mm formed the reservoir for the high-purity molten solder. The reservoir held the molten solder, which was disturbed on-demand by the activated stroke of a submerged disk-shaped piston. The outer wall of the reservoir was wrapped in resistance heaters to maintain the solder melt at 210°C (melting point of 183°C) during the tests. On top of the heaters, insulating silicone tape was attached to minimize heat losses. A thermocouple attached to the outer surface of the reservoir was used to monitor the solder temperature in real time. Each droplet was jetted by the forced displacement of the vertically moving piston. Upon such activation, a small amount of solder escaped by the orifice, thus forming a droplet. The velocity of the piston was modulated by a crank rocker mechanism, thus providing control over the exit velocity of the droplet.

The environmental chamber was a transparent rectangular airtight vessel constructed of Plexiglas. During the experiments, the environmental chamber was continuously purged with a gentle flow of nitrogen gas, to minimize solder surface degradation attributed to oxygen adsorption occurring in oxygen-containing atmospheres (Passerone et al., 1990). The oxygen content of the chamber was maintained below 20 ppm during the experiments, as confirmed by the readings of an oxygen analyzer attached to the chamber outflow port. Within this chamber, a horizontal translation stage was used to move an impacted droplet out of the field of view in preparation of the arrival of the next droplet on an unoccupied spot of the substrate. The silicon wafer substrate used in all deposition experiments was provided by Motorola and had average roughness and thickness of 0.4–0.6 Å and 0.35 mm, respectively. No further surface preparation was performed after the substrate

Table 1. Data for All Impact Cases Considered in This Study

Session	D_o (mm)	V_o	Re	We	Fr	Bo	Oh ($\times 10^3$)	D_m (mm)	D_m/D_o Normalized	D_m/D_o [1]**	D_m/D_o [2]**	D_m/D_o [3]**	E^* [3]**
326	1.11	0.96	3336.9	24.32	84.66	0.29	1.48	2.13	1.92	1.69	2.22	2.24	−0.033
327	0.99	0.86	2654.2	17.25	75.51	0.23	1.56	2.04	2.07	1.52	2.05	2.04	0.020
333	1.00	0.85	2651.3	17.10	73.89	0.23	1.56	2.03	2.04	1.52	2.05	2.04	0.008
334	0.93	0.82	2392.3	14.84	72.87	0.20	1.61	2.02	2.16	1.46	1.98	1.96	0.068
335	0.94	0.92	2714.8	18.98	91.91	0.21	1.60	2.06	2.19	1.56	2.09	2.09	0.076
336	1.01	0.85	2703.2	17.44	72.47	0.24	1.54	2.05	2.02	1.53	2.05	2.05	0.003
342	0.97	0.79	2396.8	14.40	66.02	0.22	1.58	2.00	2.07	1.44	1.97	1.95	0.021
344	0.94	0.86	2514.9	16.35	79.69	0.20	1.61	2.03	2.16	1.49	2.02	2.01	0.062
346	1.06	0.89	2953.4	19.92	75.87	0.26	1.51	2.06	1.95	1.59	2.12	2.13	−0.023
359	1.22	1.36	5191.7	53.68	155.45	0.34	1.41	3.02	2.48	2.24	2.73	2.79	0.211
361	1.00	1.11	3472.2	29.23	125.49	0.23	1.56	2.10	2.10	1.80	2.31	2.35	0.037
364	0.88	1.23	3389.1	31.54	173.59	0.18	1.66	2.22	2.52	1.84	2.35	2.39	0.230
365	0.93	1.14	3341.7	28.96	142.17	0.20	1.61	2.07	2.22	1.79	2.30	2.34	0.091
371	0.92	1.14	3306.8	28.66	143.67	0.20	1.62	2.06	2.23	1.79	2.30	2.33	0.098
372	1.01	1.31	4141.6	41.19	173.43	0.24	1.55	2.34	2.32	2.03	2.52	2.58	0.133
391	0.76	1.10	2613.4	21.75	161.11	0.13	1.78	1.68	2.21	1.63	2.14	2.15	0.085
393*	0.87	1.11	3024.4	25.51	144.90	0.18	1.67	—	—	—	—	—	—
395*	0.73	1.10	2516.5	20.95	167.32	0.13	1.82	—	—	—	—	—	—
396	0.99	1.10	3401.7	28.32	123.78	0.23	1.56	2.09	2.12	1.78	2.30	2.33	0.042
397	1.11	1.13	3934.1	33.85	118.17	0.29	1.48	2.17	1.96	1.89	2.41	2.45	−0.021
398	0.92	1.13	3259.3	27.86	139.87	0.20	1.62	2.03	2.20	1.77	2.28	2.31	0.083
402	0.85	1.18	3170.1	28.51	167.57	0.17	1.68	1.88	2.20	1.78	2.29	2.32	0.085
403	1.34	1.30	5464.0	53.80	231.08	0.42	1.17	2.93	2.38	2.18	2.33	2.80	0.121

Note: The droplets consisted of molten Sn/Pb solder; the substrate was a silicon wafer at room temperature.
*D_m measurements not possible.
**[1] Fukai et al. (1998); [2] Aziz and Chandra (2000); [3] Mao et al. (1997b).

was produced by chemical vapor deposition. The substrate was at room temperature during all experiments.

A high-speed digital video camera (Kodak HRC; 1000 frames/s), equipped with a microscope lens, was used to visualize and digitally store each droplet impact event. The impact was backlit using a fiber-optic light source. The camera recorded images on an array of 512 × 384 pixels in black and white. A second video camera (Redlake Motion Pro, 10,000 frames/s; Redlake, San Diego, CA) was also used for limited dynamic contact angle measurements (resolution 1280 × 168 in black and white). Only partial view was used for the contact angle measurements because only the area in the vicinity of the contact line was of interest.

The jetting of high-purity 63%Sn–37%Pb eutectic solder showed that spherical droplets of predictable diameter and velocity could be produced with this apparatus. Depending on piston activation, impact diameters D_o ranged from 0.7 to 1.4 mm, whereas impact velocities V_o ranged from 0.7 to 1.4 m/s. Using the solder property values listed in Xiong et al. (1998), the corresponding Reynolds number ($\mathrm{Re} = V_o D_o/\nu$, where ν is the kinematic viscosity of the liquid) and Weber number ($\mathrm{We} = \rho V_o^2 D_o/\gamma$, where γ is the surface tension of the liquid) are of $O(1000)$ and $O(10)$, respectively. Table 1 lists the impact conditions for all cases considered herein along with the corresponding values of Re and We. Each impact event is identified by a session number in this table (first column). Dark shading indicates those cases where partial rebound occurred. The corresponding values of Froude number ($\mathrm{Fr} = V_o^2/D_o g$), Bond number [$\mathrm{Bo} = \rho(gD^2/\gamma)$], and Ohnesorge number [$\mathrm{Oh} = \mu/(\rho\gamma D_o)^{0.5}$] are also listed in Table 1. It is seen that Fr = $O(10–100)$, Bo = $O(0.1)$, and Oh = $O(0.001)$. Based on the analysis of Schiaffino and Sonin (1997b), the ratio of time scales for viscous diffusion τ_{visc} and inertial oscillations τ_{osc} is $\tau_{visc}/\tau_{osc} = 1/\mathrm{Oh} = O(1000)$, meaning that inertial effects dominate viscosity, especially during the early stages, which are of specific interest in the current study. Nonetheless, it is recognized that the effects of viscosity may be important in the vicinity of the spreading contact line (Marsh et al., 1993; Schiaffino and Sonin, 1997a).

Results and Discussion

The values of maximum spreading diameter D_m, as determined in each impact event by high-speed imaging and subsequent image analysis, are listed in Table 1. Because molten solder does not wet the silicon substrate (that is, contact angles $> 90°$), D_m does not generally coincide with the maximum contact (base) diameter. This is clearly seen in the fourth frame of Figure 1, which corresponds to $t = 2.7$ ms. The column labeled D_m/D_o in Table 1 lists the normalized value of this quantity with respect to preimpact diameter. Only in two of the listed cases (sessions 393 and 395), the measurement of D_m was not possible because of visualization limitations (partial view). Nonetheless, both of these cases resulted in partial rebound, and were thus retained in the database. It is worth noting that all cases of partial rebound corresponded to Fr > 144. Because Fr scales the importance of inertia compared to gravity, and impact is in the direction of the gravitational vector, it is physically expected that partial rebound occur only when the inertia forces overwhelm gravity. However, a partial rebound criterion based solely on the value of Fr disregards the influence of surface tension, viscosity, and solidification, thus diminishing the significance of a Froude-based criterion.

Table 1 lists three additional columns of D_m/D_o values. These correspond to the predictions of the respective correlations given in Fukai et al. (1998) ([1]), Aziz and Chandra (2000) ([2]), and Mao et al. (1997b) ([3]). The correlation of Fukai et al. (1998) is given by

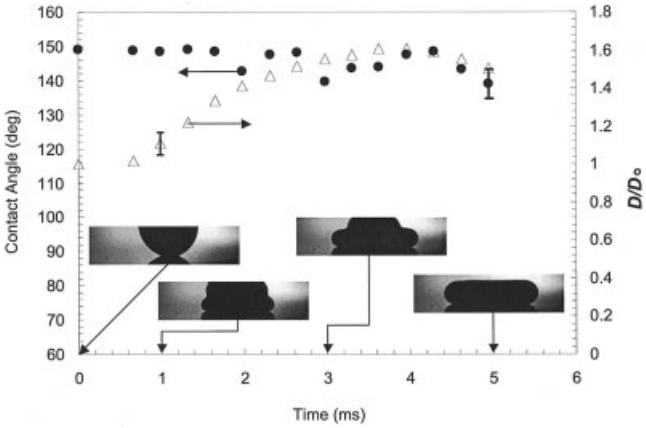

Figure 2. Temporal variation of apparent advancing contact angle and normalized spreading diameter during impingement of a 1.23-mm-diameter molten Sn/Pb solder droplet at 0.95 m/s onto a cool Si substrate.

The error bars are characteristic of all measurements for each data set. The four picture insets are actual images from the experiment corresponding to the times marked by arrows on the horizontal axis. Each picture shows mirroring of the droplet into the substrate.

$$\frac{\mathrm{We}}{2\mathrm{Re}^{0.772}} D_m^4 + 2.29(1 - \cos\theta_a) D_m^2 - \left(\frac{\mathrm{We}}{3} + 4\right) = 0 \quad (1)$$

where θ_a denotes the *dynamic* advancing contact angle. In principle, dynamic contact angles vary with time. A separate experiment was performed to determine an appropriate value of this quantity for the molten-metal impact conditions investigated herein. To attain maximum spatial and temporal resolution in the contact line region, a higher-quality digital camera (Redlake) was used at a recording speed of 3,000 fps. Using this camera, the temporal variations of apparent contact angle θ_a and spreading diameter D were measured during impingement of a 1.23-mm-diameter solder drop at 0.95 m/s onto the Si substrate (Re = 3725, We = 27, Fr = 73.7, Bo = 0.36, Oh = 1.4×10^{-3}). This droplet did not rebound, and its measured $\theta_a(t)$ variation is shown in Figure 2 along with the corresponding values of $D/D_o(t)$. The contact angle data reveal that, during the initial spreading stage, the values of θ_a remain in the range 140–150°. Consequently, the value $\theta_a = 145°$ was used in Eq. 1 to solve for D_m, and produce the corresponding D_m/D_o column in Table 1. It can be seen that the model of Fukai et al. (1998) consistently underestimates (by an average of 20%) the experimentally determined values of D_m/D_o. This substantial discrepancy may be partially attributed to the isothermal nature of this model. Figure 2 also includes four insets showing the droplet shape at four different instances of the impact sequence used to measure $\theta_a(t)$. The severe deformation of the droplet free surface as well as the contact-line region can be visualized in these images, which correspond to the first spreading cycle, and represent shape deformation extremes throughout the entire impact process. It is worth noting that the droplet spreading time in Figure 2 (about 4 ms) is consistent with the capillarity-driven, inertially resisted spreading time scale $(\rho D_o^3/2\sigma)^{1/2} = 4.7$ ms corresponding to these specific impact conditions.

The correlation of Aziz and Chandra (2000) is also a function of the advancing contact angle θ_a

$$\frac{D_m}{D_o} = \sqrt{\frac{\mathrm{We} + 12}{\mathrm{WeSte}\sqrt{\dfrac{3k_w\rho_w C_w}{2\pi\,\mathrm{Pe}\,k_d\rho_d C_d}} + 3(1 - \cos\theta_a) + \dfrac{4\mathrm{We}}{\sqrt{\mathrm{Re}}}}} \quad (2)$$

where the subscripts w and d indicate wall or droplet properties, respectively; k is the thermal conductivity; C is the heat capacity; the Stefan number $\mathrm{Ste} = C_d(T_m - T_w)/H_f$; T_m is the melting temperature; H_f is the latent heat of fusion; and the Peclet number $\mathrm{Pe} = V_o D_o \rho_d C_d/k_d$. For the materials applicable to this study (molten solder and silicon substrate): $\rho_w = 19{,}300$ kg/m^3, $C_w = 129$ J kg^{-1} K^{-1}, $k_w = 317$ W/mK, $\rho_d = 8218$ kg/m^3, $C_d = 238$ J kg^{-1} K^{-1}, $k_d = 25$ W/mK, and $H_f = 42{,}000$ J/kg. The value $\theta_a = 145°$ was used in Eq. 2 to produce the values listed under the corresponding D_m/D_o column in Table 1. The model of Aziz and Chandra (2000) appears to track the experimentally measured values of D_m/D_o within 3% (on average). Contrary to the other two models considered herein, and which are based on isothermal flow assumptions, Eq. 2, which was developed for molten-metal drops, performs better for the nonisothermal conditions of this study.

Finally, the correlation of Mao et al. (1997b) is given by

$$\left[\frac{1}{4}(1 - \cos\theta) + 0.2\frac{\mathrm{We}^{0.83}}{\mathrm{Re}^{0.33}}\right]\left(\frac{D_m}{D_o}\right)^3 - \left(\frac{\mathrm{We}}{12} + 1\right)\frac{D_m}{D_o} + \frac{2}{3} = 0 \quad (3)$$

where θ is the static (equilibrium) contact angle. Designating an appropriate value of θ for the materials studied herein (solder on Si) presented a challenge because the molten solder cannot maintain its liquid character at the temperature of the substrate (21°C). Two separate sets of experiments were performed to resolve this issue. First, a single impact was visualized for a droplet of $D_o = 1.25$ mm impinging with $V_o = 0.12$ m/s on the silicon substrate. This low-energy impact was recorded at 3,000 fps, and the dynamic contact angle was measured on each captured frame, as done in the case of Figure 2. Figure 3 shows the temporal variation of the measured contact angle, which seems to oscillate in the narrow range between 111 and 117°, before it levels off at about 111°, indicating a sessile state thereafter. Because this particular event corresponds to very low impact energy, it is argued that it simulates near-equilibrium conditions, suggesting that the value of θ for this droplet is in the range 111–117°. To determine whether this contact angle range varies with droplet size, another set of experiments was performed with droplet diameters in the range 0.25–1.2 mm and impact velocities as low as possible. The results are listed in Table 2, which presents the measured value of the final contact angle for each droplet. This value is rather insensitive to droplet size, being in a narrow range (110–116°) in all cases. Based on the results of Figure 3 and Table 2, the value of $\theta = 113°$ was used in Eq. 3 as the appropriate equilibrium angle for the cases investigated in this study. The values of D_m/D_o, as calculated from Eq. 3, are

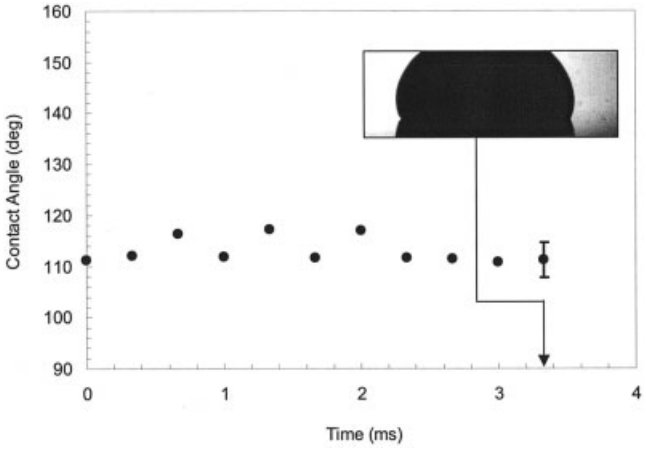

Figure 3. Temporal variation of apparent contact angle during impingement of a 1.25-mm-diameter molten Sn/Pb solder drop at 0.12 m/s onto a cool Si substrate.

The error bar is characteristic of all points. The inset shows an experimental image corresponding to $t = 3.3$ ms.

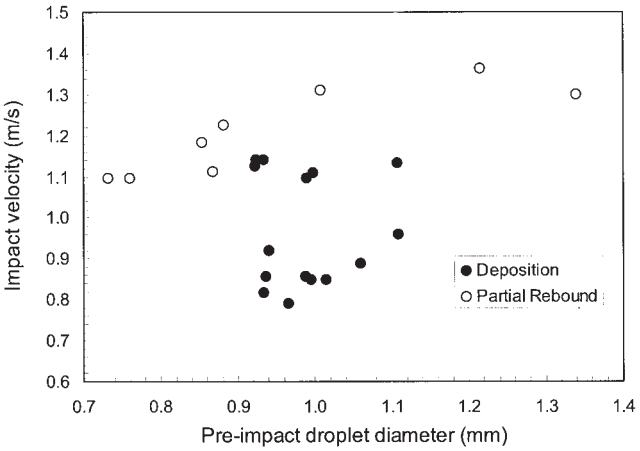

Figure 4. Impact velocity (V_o)–droplet diameter (D_o) data pairs for all impact cases investigated herein.

Solid symbols indicate deposition upon impact, whereas open symbols correspond to partial rebound (see Figure 1).

listed in Table 1 under the respective column heading. Despite its recognized limitations at impact velocities below 1 m/s, the model of Mao et al. (1997b) seems to track the experimentally measured values of D_m/D_o within an average deviation of 4%. The good agreement between the experimental data and the predictions of Aziz and Chandra (2000) and Mao et al. (1997b) is attributed to the applicability of the flat disk assumption made by both of these models. The flat disk assumption appears to be valid for the spreading phase of the impact cases considered herein, as seen by the drop shapes in Figure 2.

It is worth noticing the considerable difference between the contact angles of the nearly identical size droplets in Figure 2 (inertia-dominated) and Figure 3 (low impact energy), demonstrating the critical influence of impact momentum on fluid accumulation near the contact-line region. The added momentum in the inertia-dominated sequence of Figure 2 forces the fluid near the contact line closer to the wall, thus supporting contact angles that far exceed their counterparts in the low momentum impact of Figure 3. Further differences between the impacts of Figures 2 and 3 are discussed below.

To delineate the influence of preimpact kinematics on the droplet/wall collision outcome, impact velocities V_o and droplet diameters D_o for all cases listed in Table 1 are drawn in Figure 4 using different symbols for the two possible outcomes (deposition, partial rebound). It can be seen that under the conditions investigated herein, partial rebound is more probable at higher velocities or smaller droplet diameters. Increased impact velocities lead to increased maximum lateral spread, which, in turn, leads to increased energy available for recoil or rebound. On the other hand, as reported by Mao et al. (1997b), at higher impact velocities, increased wall shear over the extended liquid–solid contact area results in a corresponding increase of viscous dissipation, which tends to suppress recoil/rebound. As Figure 4 indicates, for higher impact velocities the increased energy overcomes the increased viscous dissipation, thus promoting the likelihood of partial rebound. This is consistent with the statement made earlier that viscous forces have a negligible effect on the early spreading/recoiling cycle of the droplets investigated herein. The higher tendency of the smaller droplets (at constant velocity) to partially rebound can be explained by considering the influence of gravity, and its resistance to the upward fluid motion during recoiling (see Figure 1). The Bond number, which is about $O(0.1)$, scales the relative importance of gravity compared to surface tension. Consequently, and as seen in Table 1 for the nine impact cases with $V_o \sim 1.1$ m/s, droplets with smaller diameters (that is, Bo < 0.2, or negligible effect of gravity) tend to break up compared to the cases where the Bond number is higher.

Table 2. Equilibrium (Static) Contact Angle of Sn/Pb Solder Droplets Deposited Gently on a Cold Si Substrate

Droplet Diameter (mm)	Static Contact Angle (deg)
0.25	116
0.50	110
0.67	113
0.75	110
1.20	112

Figure 5, which depicts the same data set on the We–Oh plane, shows that partial rebound is more likely when Oh or We increase. The values of Oh $\sim O(10^{-3})$ are indicative of the minimal global influence of viscosity (Schiaffino and Sonin, 1997b), at least for the duration of the first spreading/recoiling cycle, which is the focus of the current study. Given that higher values of We correspond to increased spreading, the higher energy available for recoil/rebound translates into an increased probability for rebound at these conditions.

Mao et al. (1997b) formulated a quantitative threshold for *isothermal* droplet rebound, which was expressed in terms of the excess rebound energy E^* defined by

$$E^* = 0.25(D_m/D_o)^2(1 - \cos\theta) - 0.12(D_m/D_o)^{2.3} \times (1 - \cos\theta)^{0.63} + \frac{2D_o}{3D_m} - 1 \quad (4)$$

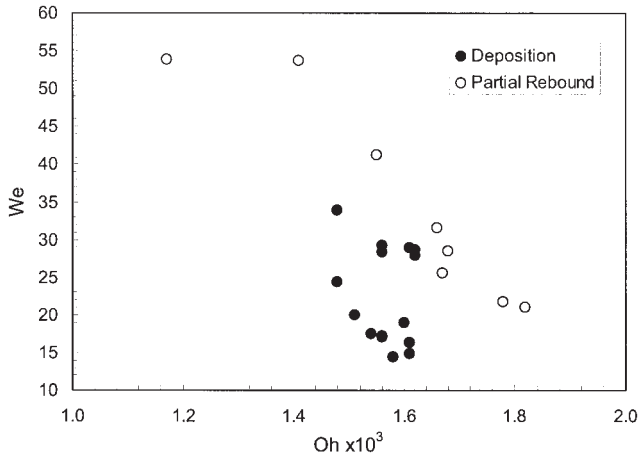

Figure 5. Weber number (*We*)–Ohnesorge number (*Oh*) data pairs for all cases investigated herein.

Solid symbols indicate deposition upon impact, whereas open symbols correspond to partial rebound (see Figure 1).

where θ denotes the *static* contact angle. The sign of the above quantity was shown to reliably predict the tendency of a droplet to deposit or rebound upon impact. Specifically, $E^* > 0$ corresponded to rebound after the first spreading/recoil cycle, whereas $E^* < 0$ corresponded to deposition. Partial rebound was *not* considered in the analysis on which the derivation of Eq. 4 was based. The value of E^* for each impact event in Table 1 was calculated from Eq. 4 using the applicable equilibrium contact angle $\theta = 113°$ and the respective *measured* values of D_m/D_o. The column labeled E^* in Table 1 lists the resulting values, which are also plotted in Figure 6 as a function of the maximum spreading ratio D_m/D_o. Different symbols reflect different outcomes (deposition or partial rebound) in this figure. Each data point in Figure 6 includes two error bars; the horizontal one represents uncertainty in determining the ratio

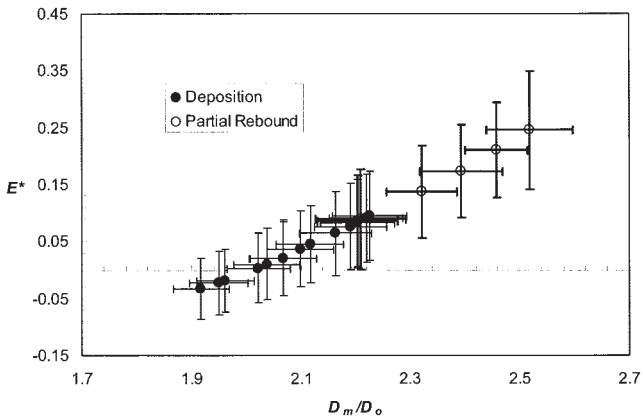

Figure 6. Excess rebound energy (Mao et al., 1997b) vs. maximum lateral spread for all cases listed in Table 1.

The horizontal error bars represent uncertainty in the ratio D_m/D_o, whereas the vertical error bars represent uncertainties in E^* from the measurement of D_m/D_o and θ. Equation 4 was used to calculate the error in E^*. For visualization purposes, the error bars for the partial rebound cases (open circles) have been drawn using thicker lines.

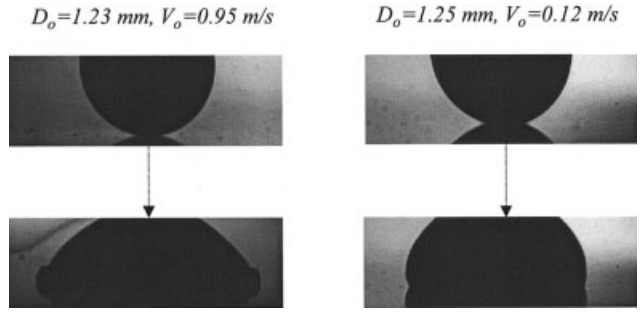

Figure 7. Preimpact (all-liquid) and solidified shapes of two Sn/Pb droplets impinging on a flat, smooth, unyielding silicon substrate.

The two droplets have identical sizes, but different velocities (both marked above the top frame of each column). Note the different shapes of the solidified deposits. Mirroring of the droplet into the substrate is apparent in each image.

D_m/D_o from the digitized images, whereas the vertical one represents uncertainty in E^* from the measurement of D_m/D_o and θ. Equation 4 was used to calculate the error in E^*, using the analysis presented by Kline and McClintock (1958) and the respective errors in D_m/D_o and θ. Figure 6 indicates that within experimental uncertainty, nearly all deposition impacts (solid circles) correspond to $E^* = 0$. Some isolated cases in this category (deposition) do correspond to small positive values of E^*, for reasons that could be attributed to the nonisothermal nature of the present study. Specifically, solidification could affect the impact outcome. For a droplet that is near the threshold between deposition and partial rebound (E^* small but positive), solidification could promote deposition under conditions that otherwise (that is, isothermal impact) would result in partial rebound. This may be one reason that the critical threshold of E^* for partial rebound seems to be slightly above zero in Figure 6. On the other hand, the impacts with partial rebound in Figure 6 (open circles) all have $E^* > 0$. The above results suggest that, although the predictive model of Mao et al. (1997b) was formulated for *complete* rebound, it can closely predict *partial* rebound as well, at least under the impact conditions investigated herein (Table 1). Furthermore, the overall applicability of the isothermal-impact criterion of Mao et al. (1997b) in the nonisothermal cases of the present study indicates that solidification has little influence on the primary metric affecting E^* (see Eq. 4), that is, maximum spreading ratio D_m/D_o. For this to be valid, solidification should not critically influence contact-line motion up to the instant of maximum spreading. In support of this inference, the molten Sn/Pb solder droplets examined herein were observed to oscillate for time periods of about 30–45 ms after impact, indicating that bulk solidification times are significantly longer than the duration of the first oscillation cycle (few milliseconds), which designates maximum spreading, and which, in turn, critically affects partial rebound.

Although the effect of solidification during the initial spreading of molten solder drops on cool Si substrates was deemed to be secondary, its overall influence on subsequent stages of the impact and the final (solidified) shape of the droplet could be important. Figure 7 shows the first ($t = 0$; all-liquid) and last ($t = \infty$; all-solid) image for each of the impact sequences corresponding to Figure 2 (inertia-dominated) and Figure 3

(near-equilibrium). Before contact with the wall, the two droplets are nearly identical in size (1.23 vs. 1.25 mm), but strike the substrate with disparately different energies. The base diameter of the solidified higher-energy droplet—as measured in Figure 7—is nearly identical to its maximum spread D_m/D_o = 1.6, which occurs at t = 3.7 ms (see Figure 2). This observation supports the hypothesis that the molten-metal droplet initially spreads, eventually attaining maximum diameter, and its contact line is arrested by freezing soon after the instant of maximum spreading. The protruding lip around the base of the higher-energy droplet in Figure 7 further supports this hypothesis. Despite the formation of the thin solidified layer at the base of the droplet early on, the remaining bulk fluid keeps oscillating until solidification is complete and the final shape of the droplet is attained. The higher energy droplet in Figure 7—as opposed to the one on the right column of the same figure—is characteristic of the impact conditions examined herein (Table 1). Thus, in nearly all cases considered in Table 1, solidification was the main factor responsible for contact-line arrest at the end of the initial spreading stage. As suggested by the applicability of the rebound criterion based on the sign of E^*, the formation of the thin solidified layer at the bottom of the oscillating droplet does not seem to have an effect on partial rebound, which occurs at the top of the droplet (far from the solidified layer) and only a few milliseconds after contact-line arrest (onset of solidification). It is apparent from Figure 7 that the two solidified droplet shapes are dissimilar, with the higher-energy impact clearly showing a wider lateral spread compared to that of the low-energy case (D/D_o = 1.61 vs. 1.27). It is thus concluded that, although solidification does not play an influential role in the early stages of spreading, it critically affects the final shape of the solidified droplet depending on impact conditions.

The capability of predicting droplet impact outcome is desired in numerous technological applications (Rioboo et al., 2001). The sign of the excess rebound energy E^* seems to offer a criterion for attaining this goal, at least under the conditions investigated herein. According to Eq. 4, the value of E^* depends only on two quantities: maximum lateral spread D_m/D_o and static contact angle θ. Consequently, the capability to predict impact outcome translates into predicting (or measuring) D_m/D_o and θ. The latter quantity can be measured experimentally, whereas the maximum spreading ratio can be determined using an existing correlation. For the impact conditions investigated in the present study and as seen in Table 1, the correlations of Aziz and Chandra (2000) and Mao et al. (1997b) provide a reliable tool because they closely predict D_m/D_o.

Conclusions

This study concentrated on droplet/wall impact conditions, which result in *partial* rebound (see Figure 1). This collision outcome has not attracted attention so far, and may be viewed as a transition stage between deposition and complete rebound, both of which have been investigated extensively in the recent past. The experiments performed in this work included high-speed digital imaging, which facilitated temporal measurements of droplet lateral spread and apparent contact angles. High-purity 63%Sn–37%Pb molten eutectic solder was the droplet material, whereas the wall consisted of a smooth, flat, unyielding silicon substrate. The solder partially wetted this substrate, as indicated by measured equilibrium and average dynamic contact angles of θ = 113° and θ_a = 145°, respectively. Droplet diameters ranged from 0.7 to 1.4 mm, whereas impact velocities ranged from 0.7 to 1.4 m/s. These conditions correspond to Re = O(1000), We = O(10), Fr = O(10–100), Bo = O(0.1), and Oh = $O(10^{-3})$.

The measured values of maximum lateral spread were compared to the predictions of three separate models (Aziz and Chandra, 2000; Fukai et al., 1998; Mao et al., 1997b), capable of providing estimates of this quantity. Good agreement between experiments and the last two of these models was shown. Partial rebound was found to be favored at higher impact velocities and smaller droplet diameters. The rebound model of Mao et al. (1997b), which was formulated for isothermal conditions, was found to offer a reliable predictor of impact outcome (deposition vs. partial rebound) under the nonisothermal conditions investigated in the present work. Finally, solidification was found to play only a minor role in the early stages of droplet spreading, but caused contact-line arrest shortly thereafter. The thin solidified layer, formed early at the bottom of the droplet, did not seem to affect partial rebound in this parameter regime. Despite this success in predicting drop/wall collision outcome in nonisothermal situations, more studies are necessary to establish the applicability of this model in other situations.

Acknowledgments

This work was supported by NASA Grants NAG3-1905 and NAG3-2456. The substrates were provided by Motorola, Inc. A. Sawczuk made contributions to the design of many experimental components and was responsible for their construction.

Literature Cited

Aziz, S. D., and S. Chandra, "Impact, Recoil and Splashing of Molten Metal Droplets," *Int. J. Heat and Mass Transfer*, **43**, 2841 (2000).

Bergeron, V., D. Bonn, J. Y. Martin, and L. Vovelle, "Controlling Droplet Deposition with Polymer Additives," *Nature*, **405**, 772 (2000).

Boomsma, K. S., "Contact Angle Dynamics in Molten Metal Droplet Impact on Flat Substrates," MS Thesis, University of Illinois at Chicago, Chicago, IL (1999).

Fukai, J., M. Tanaka, and O. Miyatake, "Maximum Spreading of Liquid Droplets Colliding with Flat Surfaces," *J. Chem. Eng. Jpn.*, **31,** 456 (1998).

Hayes, D. J., D. B. Wallace, M. T. Boldman, and R. E. Marusak, "Picoliter Solder Droplet Dispensing," *Int. J. Microcircuits and Electronic Packaging*, **16**, 173 (1993).

Klein, J., "Smart Polymer Solutions," *Nature*, **405**, 745 (2000).

Kline, S. J., and F. A. McClintock, "Describing Uncertainties in Single-Sample Experiments," *Mechanical Engineering*, American Society of Mechanical Engineers, Fairfield, NJ, p. 3 (Jan. 1958).

Mao, T., D. C. S. Kuhn, and H. Tran, "Laboratory Study of Carryover Deposition in Kraft Recovery Boilers," *J. Pulp and Paper Sci.*, **23**, J565 (1997a).

Mao, T., D. C. S. Kuhn, and H. Tran, "Spread and Rebound of Liquid Droplets upon Impact on Flat Surfaces," *AIChE J.*, **43**, 2169 (1997b).

Marsh, J. A., S. Garoff, and E. B. Dussan V, "Dynamic Contact Angles and Hydrodynamics Near a Moving Contact Line," *Phys. Rev. Lett.*, **70**, 2778 (1993).

Mundo, C., M., Sommerfeld, and C. Tropea, "Droplet-Wall Collisions: Experimental Studies of the Deformation and Breakup Process," *Int. J. Multiphase Flow*, **21**, 151 (1995).

Passerone, A., E. Ricci, and R. Sangiorgi, "Influence of Oxygen Contamination on the Surface Tension of Liquid Tin," *J. Mater. Sci.*, **25**, 4266 (1990).

Rein, M., "Phenomena of Liquid Drop Impact on Solid and Liquid Surfaces," *Fluid Dynamics Res.*, **12**, 61 (1993).
Rioboo, R., M. Marengo, and C. Tropea, "Time Evolution of Liquid Drop Impact onto Solid, Dry Surfaces," *Experiments in Fluids*, **33**, 112 (2002).
Rioboo, R., C. Tropea, and M. Marengo, "Outcomes from a Drop Impact on Solid Surfaces," *Atomization and Sprays*, **11**, 155 (2001).
Schiaffino, S. and A. A. Sonin, "Motion and Arrest of a Molten Contact Line on a Cold Surface: An Experimental Study," *Physics of Fluids*, **9**, 2217 (1997a).
Schiaffino, S. and A. A. Sonin, "Molten Droplet Deposition and Solidification at Low Weber Numbers," *Physics of Fluids*, **9**, 3172 (1997b).
Waldvogel, J. M., G. Diversiev, D. Poulikakos, C. M. Megaridis, D. Attinger, B. Xiong, and D. B. Wallace, "Impact and Solidification of Molten-Metal Droplets on Electronic Substrates," *J. Heat Transfer*, **120**, 539 (1998).
Worthington, A. M., "On the Forms Assumed by Drops of Liquids Falling Vertically on a Horizontal Plate," *Proc. R. Soc. Lond.*, **25**, 261 (1876).
Xiong, B., C. M. Megaridis, D. Poulikakos, and H. Hoang, "An Investigation of Key Factors Affecting Solder Microdroplet Deposition," *J. Heat Transfer*, **120**, 259 (1998).

Manuscript received May 12, 2003, revision received Aug. 27, 2003, and final revision received Nov. 11, 2003.